

Key Points:

- The oxidative potential (OP) of mineral dust reference materials is characterized using dithiothreitol assay
- The surface area of insoluble particles strongly affects the OP of mineral dust
- The intrinsic OP of atmospheric mineral dust aerosols is comparable to that of urban aerosols

Supporting Information:

Supporting Information may be found in the online version of this article.

Correspondence to:

C. Nishita-Hara,
nishitachiharu.z@gmail.com

Citation:

Nishita-Hara, C., Kobayashi, H., Hara, K., & Hayashi, M. (2023). Dithiothreitol-measured oxidative potential of reference materials of mineral dust: Implications for the toxicity of mineral dust aerosols in the atmosphere. *GeoHealth*, 7, e2022GH000736. <https://doi.org/10.1029/2022GH000736>

Received 19 OCT 2022

Accepted 4 MAY 2023

Author Contributions:

Conceptualization: Chiharu Nishita-Hara

Formal analysis: Chiharu Nishita-Hara

Funding acquisition: Chiharu Nishita-Hara, Masahiko Hayashi



Investigation: Chiharu Nishita-Hara, Hiroshi Kobayashi

Project Administration: Chiharu Nishita-Hara

Resources: Chiharu Nishita-Hara, Hiroshi Kobayashi, Keiichiro Hara, Masahiko Hayashi

© 2023. The Authors. GeoHealth published by Wiley Periodicals LLC on behalf of American Geophysical Union. This is an open access article under the terms of the [Creative Commons Attribution-NonCommercial-NoDerivs License](https://creativecommons.org/licenses/by-nc-nd/4.0/), which permits use and distribution in any medium, provided the original work is properly cited, the use is non-commercial and no modifications or adaptations are made.

Dithiothreitol-Measured Oxidative Potential of Reference Materials of Mineral Dust: Implications for the Toxicity of Mineral Dust Aerosols in the Atmosphere

Chiharu Nishita-Hara¹ , Hiroshi Kobayashi², Keiichiro Hara^{1,3} , and Masahiko Hayashi^{1,3}

¹Fukuoka Institute for Atmospheric Environment and Health, Fukuoka University, Fukuoka, Japan, ²Division of Life and Environmental Sciences, University of Yamanashi, Kofu, Japan, ³Department of Earth System Science, Faculty of Science, Fukuoka University, Fukuoka, Japan

Abstract Oxidative stress is a mechanism that might raise the toxicity of mineral dust aerosols. We evaluated the oxidative potential (OP) of four reference materials (RMs) of mineral dusts using dithiothreitol assay. The OP of the water-soluble fraction of the dust RMs accounts for 40%–70% of the OP of the total fraction. The values of total and water-soluble OP normalized by the surface area of insoluble particles showed agreement among the different dust RMs. The surface area of insoluble dust particles was therefore inferred as an important factor affecting the OP of mineral dust. Using the relation between total OP and the surface area of insoluble particles of the dust RMs, we estimated the total OPs of fine and coarse atmospheric mineral dust aerosols assuming a typical particle size distribution of Asian dust aerosols observed in Japan. Mass-normalized total OPs were estimated at 44 and 23 pmol min⁻¹ μg⁻¹ for fine and coarse atmospheric mineral dust particles. They closely approximate the values observed for urban aerosols in Japan, which suggests that mineral dust plume advection can lead to a marked increase in human exposure to redox-active aerosols, even far downwind from mineral dust source regions.

Plain Language Summary Mineral dust aerosols in the atmosphere are mostly soil particles swept up from arid and semi-arid land surfaces. They can be transported long distances in the atmosphere and can affect air quality throughout large areas, even far downwind from source regions. Inhalation and exposure to mineral dust aerosols adversely affect human health. Although the mechanisms of mineral dust aerosol toxicity remain unknown, oxidative stress has been implicated as a mechanism leading eventually to adverse health effects. The oxidative potential (OP) of aerosol particles is defined as the capability of aerosol particles to induce oxidative stress. To investigate the OP of mineral dust aerosols, we evaluated the OPs of reference materials of mineral dusts using a cell-free assay called dithiothreitol assay. Then we estimated the OPs of mineral dust aerosols in the atmosphere. The intrinsic OP estimated for a long-range transported mineral dust aerosol in the atmosphere was very similar to that of urban aerosols. This finding suggests that mineral dust plume advection can engender a marked increase in human exposure to toxic aerosols, consequently inducing oxidative stress even in areas far downwind from mineral dust source regions.

1. Introduction

Mineral dust aerosols in the atmosphere mostly constitute soil particles swept up from arid and semi-arid land surfaces with little vegetation, which later become suspended on strong winds. They are the most abundant aerosol components in the atmosphere by mass, representing more than half of the total global aerosol burden (Textor et al., 2006). The most important source regions of mineral dust aerosols are the dust belt stretching through the Sahara and Sahel in North Africa, the Middle East, and southwestern and eastern Asia (Ginoux et al., 2012; Kok et al., 2021; Prospero et al., 2002). Once soil dust particles are entrained into the atmosphere, they can be transported for thousands of kilometers and can occasionally be transported even intercontinentally on hemispheric scales (Grousset et al., 2003; McKendry et al., 2007; Uno et al., 2009). Therefore, mineral dust aerosols affect air quality not only near source regions but also throughout large areas located far downwind from source regions. However, because of dispersion and deposition, the atmospheric dust concentration decreases concomitantly with increasing distance of transport. Near source regions, the mass of mineral dust aerosol particles is dominated by large particles with diameters of approximately 5–20 μm, which transition to smaller particles during atmospheric transport because the atmospheric life time of smaller dust particles is longer. Larger dust particles fall out with

Writing – original draft: Chiharu

Nishita-Hara

Writing – review & editing: Chiharu

Nishita-Hara, Hiroshi Kobayashi,

Keiichiro Hara

higher frequency because of both dry and wet deposition processes (Mahowald et al., 2014). The mean residence time for fine dust particles of less than 2.5 μm diameter is longer than 5–9 days, but it is shorter than 1–2 days for coarse dust particles with diameter greater than 10 μm (Kok et al., 2017). Mineral dust aerosols comprise a complex mixture of various mineral components such as phyllosilicate (e.g., illite, kaolinite, chlorite, biotite, and muscovite), quartz, plagioclase, calcite, feldspar, iron oxides, and dolomite (Jeong, 2008; Jeong et al., 2014; Sokolik & Toon, 1999). The relative abundance of the mineral components varies depending on the source region (Caquineau et al., 1998; Formenti et al., 2011, 2014; Sokolik & Toon, 1999) and particle size (Jeong, 2008; Jeong et al., 2014). Mineral dust aerosols are usually regarded as natural aerosols. However, anthropogenic land use and land cover changes affect mineral dust emissions (e.g., Ginoux et al., 2012). Climate change also affects the atmospheric burden of mineral dust aerosols (e.g., Mahowald et al., 1999; Stanelle et al., 2014). Furthermore, long-range transported mineral dust particles often contain sulfates or nitrates formed via heterogeneous reactions with sulfur dioxide or nitrogen oxides emitted from anthropogenic sources (e.g., Trochkin et al., 2003; Zhang et al., 2000).

The health effects of mineral dust aerosols have attracted great concern recently (Aghababaeian et al., 2021; de Longueville et al., 2013; Fussell & Kelly, 2021; Goudie, 2014; Hashizume et al., 2010, 2020; Karanasiou et al., 2012; Kotsyfakis et al., 2019; Zhang et al., 2016). Recent systematic reviews of epidemiologic studies have demonstrated that inhalation and exposure to mineral dust aerosols adversely affect human health, leading particularly to cardiorespiratory diseases (Aghababaeian et al., 2021; Hashizume et al., 2020; Kotsyfakis et al., 2019). In mouse models, mineral dust particle inhalation has induced respiratory inflammation (Hiyoshi et al., 2005; Ichinose et al., 2008). In terms of mass, mineral dust aerosols are usually predominantly coarse particles (>2.5 μm particle diameter). Coarse particles are less able to penetrate to the lungs than fine particles (0.1–2.5 μm diameter) are. However, even if mineral dust particles might not be inhaled into the lung in large quantities by mass, they still exert important health effects because the deposition efficiencies of coarse particles throughout the whole respiratory tract, especially for the upper respiratory tract and bronchial region, are much greater than those of fine particles (Hyder et al., 1986).

Although the mechanisms of mineral dust aerosol toxicity remain unknown, oxidative stress has been implicated as a mechanism causing mineral dust-induced inflammatory responses (He et al., 2019; Higashisaka et al., 2014; Kyung et al., 2012; Pardo et al., 2017). Oxidative stress is a state of imbalance between reactive oxygen species (ROS) and antioxidants in favor of the ROS in tissues and organs. When mineral dust particles are deposited in the respiratory tract, redox-active species can dissolve from mineral surfaces and can act as a catalyst of ROS formation from molecular oxygen (O_2) in the epithelial lining fluid. Moreover, surfaces of insoluble metal-containing minerals can act as a heterogeneous catalyst for ROS formation. Transition metals adsorbed onto mineral surfaces or contained in minerals as structural metals are expected to act as an electron donor in O_2 reduction (Schoonen et al., 2006).

The oxidative potential (OP) of aerosol particles is defined as the capability of aerosol particles to deplete antioxidants and to generate ROS. Dithiothreitol (DTT) assay, an acellular assay, is used widely to quantify the OP of aerosol particles (Cho et al., 2005; Jiang et al., 2019; Li et al., 2009). Using DTT as a surrogate of cellular antioxidants, DTT assay simulates aerosol particle-catalyzed electron transfer from cellular antioxidants (e.g., nicotinamide adenine dinucleotide (NADH), nicotinamide adenine dinucleotide phosphate (NADPH), glutathione, ascorbic acid, and uric acid) to O_2 and generation of superoxide radical ($\text{O}_2^{\bullet-}$) and hydrogen peroxide (H_2O_2) in body fluids (Li et al., 2009). In the assay, DTT is oxidized to its disulfide form. In fact, the DTT loss rate (OP^{DTT}) represents the measure of OP of aerosol particles. Multiple epidemiological reports, as presented in a review, have described that exposure to OP as measured by DTT assay is associated more strongly with the risk of cardiorespiratory diseases than aerosol particle mass is (Bates et al., 2019), suggesting that OP^{DTT} is a more health-relevant metric than the mass concentration of aerosol particles. Chemical species identified as DTT-active are water-soluble transition metals (e.g., Cu and Mn) (Charrier & Anastasio, 2012), quinones (Charrier & Anastasio, 2012; Kumagai et al., 2002), and metal oxides (e.g., CuO, MnO_2 , and PbO) (Nicolas et al., 2015), although other chemical species might be DTT-active. Results of atmospheric observations have indicated that mineral dust particles contribute substantial amounts of OP^{DTT} of fine and coarse aerosol particles (Q. Liu, Baumgartner et al., 2014; Q. Liu, Zhang et al., 2014; W. Liu et al., 2018; Nishita-Hara et al., 2019; Yu et al., 2019). However, the OP^{DTT} values of desert dusts have been quantified only rarely. Conte et al. (2017) reported very low DTT activity of a dust sample generated from surface soil in the Sahara Desert, which is inconsistent with results of atmospheric observations. The surface area of mineral dust particles might be an important

factor for the OP of mineral dusts because mineral surfaces reportedly work as a heterogeneous catalyst in ROS formation (Schoonen et al., 2006). In addition, water-soluble transition metals are expected to be dissolved from the surfaces of the mineral dusts (Baker & Jickells, 2006; Ooki et al., 2009; Shi et al., 2011). The specific surface areas (SSA; total surface area contained in a unit mass) of aerosol particles generally increase concomitantly with decreasing particle size. Therefore, the size distributions of mineral dust particles might affect their mass-normalized OP^{DTT} . However, the putative relations between OP^{DTT} and the surface areas of mineral dust particles have not been investigated.

Reference materials (RMs) of desert dust, such as certified RMs CJ-1 and CJ-2, the National Institute of Environmental Studies (NIES) certified RM No. 30, and Arizona Test Dust (ATD), have been used widely as surrogates of atmospheric mineral dust aerosols for studies of toxicology, cloud microphysics, atmospheric radiology, and atmospheric chemistry (e.g., Hiyoshi et al., 2005; Ichinose et al., 2008; Kameda et al., 2016; Kanji & Abbatt, 2010; Möhler et al., 2006; Osada, 2013; Park et al., 2017; Sakai et al., 2010; Tang et al., 2014; Veghte et al., 2016; Yamashita et al., 2011). However, OPs of the dust RMs have not been characterized. For the present study, to investigate OP^{DTT} of mineral dust aerosols in the atmosphere, we characterize OP^{DTT} of the total and water-soluble fractions of these mineral dust RMs. Moreover, to elucidate the relations between OP^{DTT} and the surface areas of mineral dust particles, we measure the size distributions of insoluble dust particles included in the dust RMs and estimate the respective surface areas of the insoluble dust particles. Then, based on results obtained from experimentation, we attempt to estimate OP^{DTT} of fine and coarse mineral dust aerosol particles in the atmosphere. Finally, we compare the estimated OP^{DTT} values with actual OP^{DTT} values observed for atmospheric aerosols during dust events and non-dust periods.

2. Materials and Methods

2.1. Reference Materials of Mineral Dust

For four dust samples provided as RM, we measured OP^{DTT} : (a) NIES certified RM No. 30 “Gobi Kosa dust,” (b) certified RM CJ-1 “China Loess,” (c) certified RM CJ-2 “Simulated Asian Mineral Dust,” and (d) fine grade of ATD (ISO 12103-1, A2 Fine Test Dust). Hereinafter, these dust RMs are designated respectively as No. 30, CJ-1, CJ-2, and ATD. The original soils of No. 30, CJ-1, and CJ-2 were collected respectively from the southern Gobi Desert in Mongolia and the loess plateau and the Tengger Desert in China (Nishikawa et al., 2000, 2013). These areas are known as source areas of Asian dust. The original soil of ATD was collected from the Arizona desert in the United States. After the dust RMs were generated from surface soils, they were refined by coarse sieving, cyclone classification, and homogenization. Figure S1 in Supporting Information S1 presents a summary of the elemental compositions of No. 30, CJ-1, CJ-2, and ATD based on ISO standard documentation and data provided by Nishikawa et al. (2000, 2013). The elemental compositions of the dust RMs are similar. Quartz, feldspar, and clays are identified as major mineral components for CJ-1, CJ-2, and ATD (Broadley et al., 2012; Yabuki et al., 2002). Although quantitative data of mineral components of No. 30 are not available from the related literature, X-ray diffraction patterns indicate similarity of the three RMs of Asian dust (No. 30, CJ-1, and CJ-2) (Nishikawa et al., 2013).

2.2. Size Distribution Measurement and Specific Surface Area Estimation of Water-Insoluble Dust Particles

The numbers and sizes of water-insoluble particles included in No. 30, CJ-1, CJ-2, and ATD were measured using a Coulter Multisizer™ (Multisizer-3; Beckman Coulter Inc.). Particles with diameter of approximately 1.4–160 μm were counted. Isoton™ II Diluent (Beckman Coulter Inc., pH 7.35–7.65) was used as the dispersing medium. From the measured number–size distributions, we estimated SSA of the insoluble particles according to the following explanation.

First, we estimated the total particle volume: V_{total} . Volume–size distributions were calculated from the measured number–size distributions assuming spherical particles. To include particles that are larger or smaller than the measurement size range in the calculations of V_{total} , the volume–size distributions were approximated as a sum of two or three lognormal distributions, as presented below.

$$\frac{dV}{d \log D_p} = \sum_{i=1}^n \frac{V_i}{\sqrt{2\pi \log \sigma_{g,i}}} \exp \left[-\frac{(\log D_p - \log D_{g,p,i})^2}{2 \log^2 \sigma_{g,i}} \right] \quad (1)$$

Therein, D_p stands for the particle diameter, n denotes the number of modes, $D_{g,p,i}$ is the modal geometric mean diameter, $\sigma_{g,i}$ expresses the modal geometric standard deviation, and V_i signifies the particle volume in mode i . V_{total} was obtained as

$$V_{\text{total}} = \sum_{i=1}^n V_i. \quad (2)$$

Then we calculated the total particle surface area: S_{total} . Surface–size distributions were estimated from the measured number–size distributions, assuming spherical particles. Similarly, the surface–size distributions were also approximated as a sum of two or three lognormal distributions, as shown below.

$$\frac{dS}{d \log D_p} = \sum_{i=1}^n \frac{S_i}{\sqrt{2\pi \log \sigma_{g,i}}} \exp \left[-\frac{(\log D_p - \log D_{g,p,i})^2}{2 \log^2 \sigma_{g,i}} \right] \quad (3)$$

Therein, S_i represents the surface area of particles in mode i . S_{total} was obtained as

$$S_{\text{total}} = \sum_{i=1}^n S_i. \quad (4)$$

The values of SSA were obtained as

$$\text{SSA} = \frac{S_{\text{total}}}{\rho V_{\text{total}}}. \quad (5)$$

In that equation, ρ represents the particle density. The densities of the major mineral constituents of mineral dust are quite similar (e.g., 2.55–2.76 g cm⁻³ for feldspar, 2.65 g cm⁻³ for quartz, and 2.6–2.9 g cm⁻³ for illite). Actually, density of approximately 2.5–2.6 g cm⁻³ is often assumed as the bulk density of mineral dust aerosols (e.g., Kok et al., 2017; McNaughton et al., 2007; Möhler et al., 2006). For this study, we used the density of quartz (2.65 g cm⁻³) to calculate the SSA values of the dust RMs.

We calculated S_{total} and V_{total} assuming spherical particles. However, in fact, solid dust particles are not spherical. Because the Coulter Multisizer measures the volume-equivalent size in principle, the assumption for particle shape might not engender large error for V_{total} . However, S_{total} might be underestimated considerably because of assumptions of the particle shape. The particle surface area calculated by assuming spherical particles represents the lower limit. The relative relation of SSAs of the dust RMs will be preserved if the particle shapes (i.e., aspect ratio and surface roughness) are similar among the dust RMs, although no data are available for the shapes of dust RMs.

2.3. DTT Assay

The OP^{DTT} of the total and water-soluble fractions of the dust RMs were analyzed using DTT assay in accordance with the procedure described by Cho et al. (2005). Briefly, in the assay, the loss of 100- μ M DTT in 0.10 M potassium phosphate buffer (pH 7.4) at 37°C was measured over time. To measure the DTT loss rates of the total fraction of the dust particles (OP^{DTT}_{total}), after a suspension of the dust particles in 36 ml of 0.11 M potassium phosphate buffer solution was prepared in a polypropylene amber centrifuge tube, it was sonicated for 30 min. Then, 4 ml of 1,000- μ M DTT was added to the suspended solution that had been pre-warmed to 37°C. It was shaken continuously at 400 rpm at 37°C using a dry bath incubator. At four specified times, a 0.50-ml aliquot of the incubated mixture was withdrawn and was added to 0.50 ml of 10% trichloroacetic acid in another tube (reaction tube) to terminate the reaction. Next, 0.10 ml of 5 mM dithiobisnitrobenzoic acid (DTNB) solution was added to the reaction tube, mixed, and allowed to react for 5 min. Then 2.0 ml of Tris-ethylenediaminetetraacetic acid (EDTA)-HCl buffer (0.80 M, pH 8.9) was added. The reaction of DTT and DTNB forms 2-nitro-5-thiobenzonic acid (TNB). To quantify the TNB concentration, its absorbance at 412 nm was measured using a spectrophotometer (Genesys30; Thermo Scientific). Then TNB was quantified using molar absorptivity of 14,150 M⁻¹ cm⁻¹ (Eyer et al., 2003; Li et al., 2009). The DTT loss rate was ascertained from the linear regression slope of four data points. We changed the total time of DTT assay between 15 and 90 min depending on concentrations of the dust RMs and their DTT-reactivities. The four specified times of the data points were, for example, (0, 5, 10, 15) min and (0, 30, 60, 90) min, respectively, when the total times were set as 15 and 90 min.

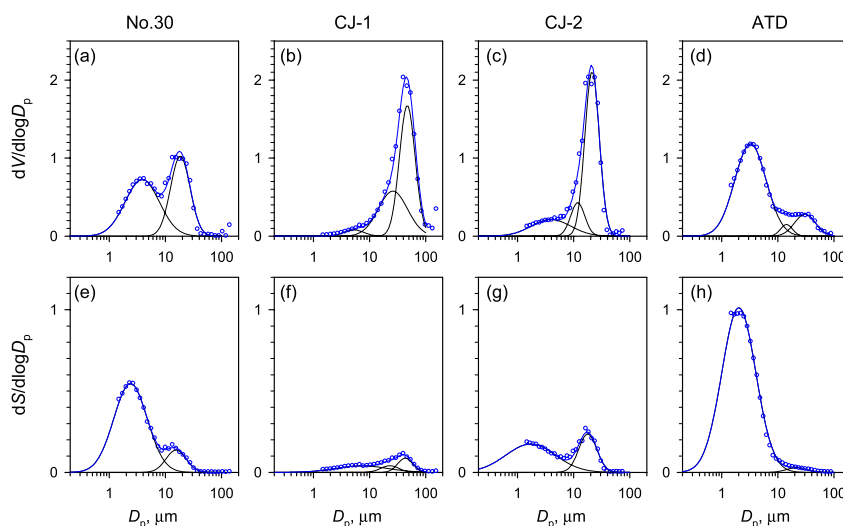


Figure 1. Volume–size and surface–size distributions of insoluble particles included in the mineral dust RMs: volume–size distribution of (a) No. 30, (b) CJ-1, (c) CJ-2, and (d) Arizona Test Dust (ATD), and surface–size distribution of (e) No. 30, (f) CJ-1, (g) CJ-2, and (h) ATD. The volume and surface areas of the particles were normalized so that the V_{total} is 1 unit volume. Blue circles represent volume–size or surface–size distribution values calculated from measurement data. Blue lines represent results of curve-fitting with the sum of lognormal distributions. Black lines show individual modes.

To measure the DTT loss rates of the water-soluble fraction of dust particles ($\text{OP}_{\text{total}}^{\text{DTT}}_{\text{ws}}$), the loss of 100- μM DTT was measured at the same condition with $\text{OP}_{\text{total}}^{\text{DTT}}$. As a pretreatment of the analysis, suspensions of the dust RMs in 0.11-M potassium phosphate buffer were sonicated for 30 min. We used the buffer solution to extract the water-soluble fraction because the solubility of metals in water depends on the pH value. The sonicated suspensions were then filtrated using a Teflon membrane filter with 0.45- μm pore size (DigiFILTER; SCP Science) to remove water-insoluble particles. Then, 1 ml of 1,000- μM DTT was added to 9 ml of the filtrate that had been pre-warmed to 37°C. Subsequently, the DTT loss rate in the filtrate was measured as $\text{OP}_{\text{total}}^{\text{DTT}}_{\text{ws}}$ using the same procedure as that used to measure $\text{OP}_{\text{total}}^{\text{DTT}}$.

A blank and a positive control were analyzed each day during the experiment. The DTT loss rate in the potassium phosphate buffer without a dust sample was negligible ($<0.01 \mu\text{M min}^{-1}$). The DTT loss rate obtained for the positive control (0.20- μM phenanthrenequinone) was reproducible with a mean (\pm standard deviation) of $2.97 \pm 0.20 \mu\text{M min}^{-1}$ ($N = 14$).

3. Results and Discussion

3.1. Size Distributions of Water-Insoluble Particles in the Mineral Dust RMs

Figure 1 depicts the volume–size and surface–size distributions of water-insoluble particles included in the dust RMs. Both the volume–size and surface–size distributions presented in Figure 1 were normalized by V_{total} . Parameters of lognormal functions obtained by fitting on the volume–size and surface–size distributions are presented respectively in Tables S1 and S2 in Supporting Information S1. Size distributions of the insoluble particles varied greatly among the dust RMs. The volume–size distribution of No. 30 (Figure 1a) showed a bimodal structure with two comparable modes at 3.9 and 18 μm diameter. However, the volume–size distributions of CJ-1 (Figure 1b), CJ-2 (Figure 1c), and ATD (Figure 1d) had a dominant mode. The dominant mode diameters were 49, 21, and 3.3 μm , respectively, for CJ-1, CJ-2, and ATD. The size distribution of ATD was the most similar to those typically observed for long-range transported mineral dust aerosols, whereas the size distributions of CJ-1 and CJ-2 were similar to those typically observed near the source regions of mineral dust aerosols (Formenti et al., 2011; Mahowald et al., 2014). The average particle size weighted by volume was $\text{CJ-1} > \text{CJ-2} > \text{No. 30} > \text{ATD}$. Because it is associated with variation of the particle size distributions, the SSAs also varied greatly among the dust RMs. The SSAs were 0.092, 0.288, 0.469, and 0.783 $\text{mm}^2 \mu\text{g}^{-1}$, respectively, for CJ-1, CJ-2, No. 30, and ATD.

The size distribution of insoluble particles is not the same as that of total particles of the dust RMs. Osada (2013) presented a volume fraction of 29% for water-soluble components in CJ-1 and 13% for that in CJ-2 as median

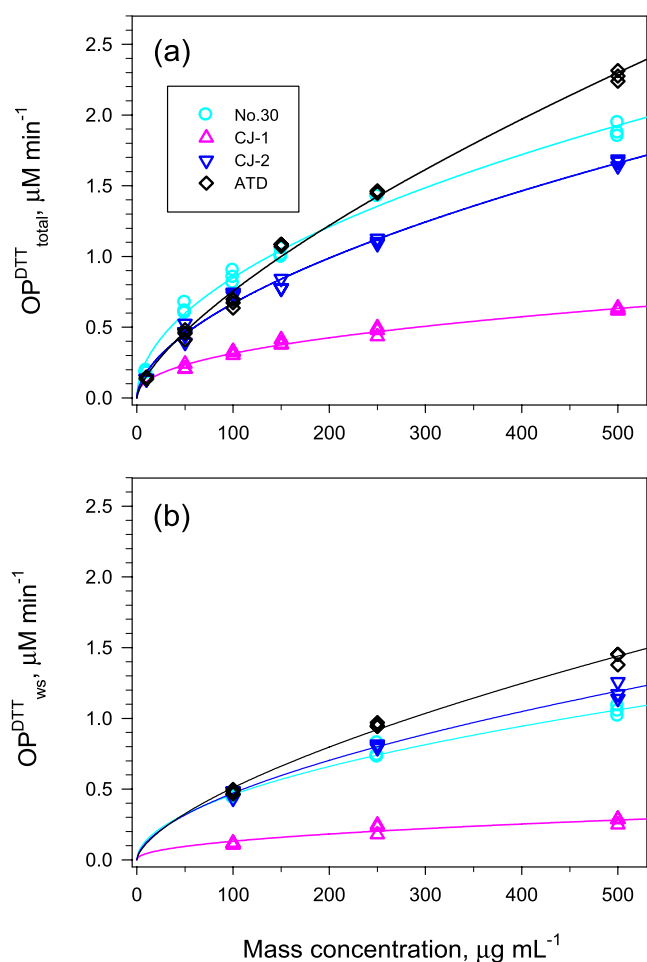


Figure 2. DTT loss rates as a function of the mass concentration of the dust reference materials (RMs) in the DTT solutions: (a) OP_{total}^{DTT} and (b) OP_{ws}^{DTT} . The x-axis represents the mass concentration of the dust RM in suspensions before filtration. The lines are regression lines.

If this non-linearity of mineral dust OP also occurs in response to antioxidants in vivo, then the health risk from mineral dust exposure might not decrease linearly even when the atmospheric dust concentration decreases at order level after long-range transport from source regions.

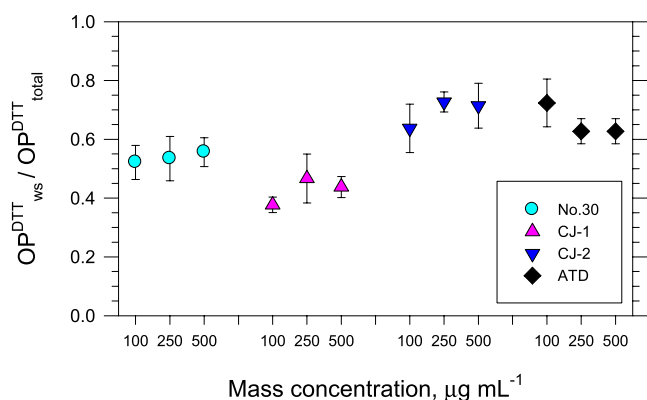


Figure 3. Fraction of OP_{ws}^{DTT} against OP_{total}^{DTT} . Error bars show two standard variations of triplicate measurements.

values with no size trend, although no data are available for No. 30 and ATD in the literature. Assuming these volume fractions of water-soluble components (13%–29%) and a core-shell particle structure, the diameters of total dust particles are estimated as 5%–10% larger than those of insoluble dust particles.

3.2. Oxidative Potential of Total and Water-Soluble Fractions of the Mineral Dust RMs

Figure 2 portrays values of OP_{total}^{DTT} and OP_{ws}^{DTT} of the dust RMs as a function of the dust mass concentration in DTT solution. The regression equations in Figure 2 are presented in Table S3 in Supporting Information S1. After normalization by the dust mass concentration, both OP_{total}^{DTT} and OP_{ws}^{DTT} were found to be the lowest for CJ-1. In addition, ATD was the highest in OP_{total}^{DTT} for the higher mass concentrations (150–500 $\mu g \text{ mL}^{-1}$) (Figure 2a). However, for the lower mass concentrations (10–100 $\mu g \text{ mL}^{-1}$), No. 30 was the highest in OP_{total}^{DTT} . Regarding OP_{ws}^{DTT} (Figure 2b), ATD was found to be the highest for all dust mass concentrations (100–500 $\mu g \text{ mL}^{-1}$). Furthermore, neither OP_{total}^{DTT} nor OP_{ws}^{DTT} was found to be linearly related to the mass concentration. Rather, they both were well-fit by a power function.

Similar nonlinear concentration-response curves were found for OP^{DTT} of Cu and Mn ions, whereas OP^{DTT} of quinones and Fe, Ni, and V ions are linear with respect to their concentrations (Charrier & Anastasio, 2012). It remains unclear why OP^{DTT} is nonlinear with respect to Cu or Mn ions concentration. According to a Cu^{2+} -catalyzed DTT oxidation mechanism proposed by Kachur et al. (1997), the Cu^{2+} -DTT complex is formed and serves as the catalysts for DTT oxidation. In that mechanism, only the un-complexed DTT can be oxidized. Consequently, at high Cu^{2+} concentration, the Cu^{2+} -DTT complex formation might result in a decrease of DTT oxidation efficiency. However, as discussed in the subsequent section (Section 3.3), contribution of Cu ion is expected to be quite small for the DTT consumption by mineral dust. Therefore, the Cu^{2+} -DTT complex formation cannot explain the nonlinear concentration-response curves of mineral dust RMs quantitatively. Additionally, it remains unclear whether the non-linearity of DTT reactivity of mineral dust RMs occurs only in the reaction with DTT or not.

As expected, comparison of OP_{ws}^{DTT} with OP_{total}^{DTT} of the same RM revealed OP_{ws}^{DTT} as invariably lower than OP_{total}^{DTT} . Figure 3 shows $OP_{ws}^{DTT} / OP_{total}^{DTT}$ ratios for each RM. The $OP_{ws}^{DTT} / OP_{total}^{DTT}$ ratios were 0.4–0.7, indicating that water-soluble and insoluble fractions of mineral dust particles contribute comparably to DTT consumption. Our earlier study (Nishita-Hara et al., 2019) revealed that water soluble transition metals (mainly Cu and Mn) can explain only approximately 60% of OP_{total}^{DTT} of the coarse particles (>2.5 μm in particle diameter) collected from Asian dust plumes in Japan, although their OP_{total}^{DTT} correlates strongly with concentrations of crustal elements (e.g., Al and Fe) in the coarse particles. Based on results of this study, water-insoluble mineral dust particles account for the residual fraction of OP_{total}^{DTT} of the coarse particles, which was not explained by transition metal ions in our earlier study. For the coarse particles in Asian dust plumes, transition metal ions and surfaces of the water-insoluble mineral dust might account for most of their OP_{total}^{DTT} .

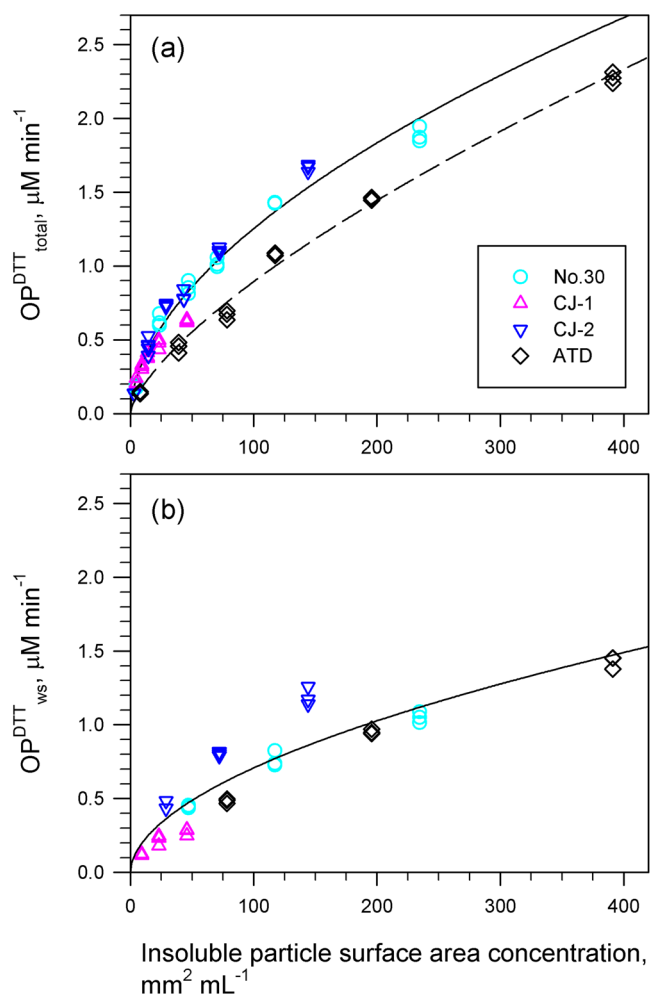


Figure 4. DTT loss rates as a function of the insoluble particle surface area concentration: (a) OP^{DTT}_{total} and (b) OP^{DTT}_{ws} . The x axis shows the surface area concentration of insoluble particles in the suspensions before filtration. The lines are regression lines. In panel a, solid and broken lines respectively represent regression lines of Asian dust reference materials (No. 30, CJ-1, CJ-2) and Arizona Test Dust.

3.3. Relation Between Oxidative Potential of the Dust RMs and Surface Area Concentration of Water-Insoluble Particles

Figure 4 presents OP^{DTT}_{total} and OP^{DTT}_{ws} of the dust RMs as a function of the surface area concentration of water-insoluble particles in the DTT solution. The regression equations in Figure 4 are presented in Table 1. Surface area concentrations of the insoluble particles were calculated from the dust masses added to the DTT solution for the DTT assay and the SSAs of insoluble particles. The calculations were made assuming that the mass of the water-soluble fraction is negligible in the dust RMs. This assumption might not be sufficiently plausible. As described in Section 3.1, volume fractions 29% and 13% were reported by Osada (2013) for the water-soluble components in CJ-1 and CJ-2. Based on the water-soluble component fractions, the surface area concentrations of insoluble particles calculated here might be overvalued by approximately 10%–30%.

Surface-area-normalized OP^{DTT}_{total} of the four dust RMs showed rough agreement (Figure 4a). Especially, surface-area-normalized OP^{DTT}_{total} for the RMs of Asian dust (No.30, CJ-1, and CJ-2) well agreed. The values can be fitted together collectively by a regression curve with a high coefficient of determination ($R^2 = 0.97$). This result indicates that the surface area of insoluble particles included in mineral dust is a crucially important controlling factor for their OP^{DTT}_{total} . After normalization by the particle surface area of insoluble particles, OP^{DTT}_{total} of ATD was lower than that of the Asian dust RMs. This lower value might be attributable to differences in the chemical or mineral compositions of the RMs. As for mineral dusts that have originated from the same source region, the relation between OP^{DTT}_{total} and the particle surface area might be able to be collapsed to a common curve because of their similar chemical and mineral compositions. However, the surface-area-normalized OP^{DTT}_{total} of mineral dust will differ depending on the surface area concentration in DTT solution because OP^{DTT}_{total} values of dust RMs were not linear to the surface area concentration.

Surface-area-normalized OP^{DTT}_{ws} values also roughly agree among all the RMs (Figure 4b), suggesting that DTT-active water-soluble species are dissolved from the surfaces of the mineral dust particles. Transition metal ions such as Fe, Mn, and Cu ions are DTT-active species that are likely to be included in the water-soluble fraction of the dust RMs. Other DTT-active species such as quinones and humic-like substances (HULIS) are unlikely to be included in the dust RMs because such organic redox-active species are adsorbed or formed on natural mineral dust surfaces during atmospheric transport (Falkovich et al., 2004; Kameda et al., 2016). Therefore, we discuss the respective contributions of Fe, Mn, and Cu ions to OP^{DTT}_{ws} below.

In mineral dusts, Fe is the most abundant transition metal (Figure S1 in Supporting Information S1). The solubility of aerosol Fe in seawater has been studied extensively because it is an important factor in the global biogeochemical cycle of Fe, which affects ocean productivity and the carbon cycle (Jickells et al., 2005; Mahowald et al., 2018). Actually, Fe is known to dissolve from the surface of desert dust particles. Its solubility is controlled primarily by the SSA of dust particles (Baker and Jickells et al., 2006; Ooki et al., 2009; Shi et al., 2011). However, the fractional solubility of Fe (percentage of dissolved to total Fe) in mineral dusts is quite low: < ca. 1% (Ooki et al., 2009; Shi et al., 2011). Moreover, Charrier and Anastasio (2012) reported that the DTT loss rates from Fe ion are linear to its concentration. If Fe ion is predominantly responsible to OP^{DTT}_{ws} of the dust RMs, then OP^{DTT}_{ws} of the dust RMs is expected to be present in a linear relation to the surface area concentration of the insoluble dust particles. However, OP^{DTT}_{ws} was not linear to the surface area concentration (Figure 4b). Rather, it was well-fitted to a power law function. These findings and the low fractional solubility of Fe suggest that Fe ion is unlikely to contribute predominantly to OP^{DTT}_{ws} of the mineral dust RM.

Table 1
Regression Equations Show the DTT Loss Rate of the Total and Water-Soluble Fractions of the Mineral Dust Reference Materials as a Function of the Surface Area Concentration of Insoluble Particles^a

Material	Range of surface area concentrations (mm ² mL ⁻¹)	Regression equation	R ²	N ^b
Total fraction				
RM of Asian dust	3–234	$y = 0.1003x^{0.5486}$	0.97	51
ATD	8–391	$y = 0.0369x^{0.6922}$	0.99	18
Water-soluble fraction				
All	9–391	$y = 0.0598x^{0.5368}$	0.86	36

^aIn the regression equations, y represents the DTT loss rate ($\mu\text{M min}^{-1}$); x denotes the surface area concentration of insoluble particles (mm² mL⁻¹) in the DTT solution. ^b N stands for the number of independent measurements. The DTT loss rate measurements were repeated three times independently for each concentration.

Also, Mn is known to dissolve from the desert dust (Mahowald et al., 2018). The elemental concentrations of Mn in the dust RMs are lower than those of Fe by approximately one order of magnitude (Figure S1 in Supporting Information S1). However, the fractional solubility of Mn in mineral dusts is much higher (ca. 50%) (Baker et al., 2006) than that of Fe (< ca. 1%). In addition, the relation between DTT loss from Mn-ion and its concentrations follows a power law (Charrier & Anastasio, 2012). Consequently, Mn ion might be mainly responsible for OP^{DTT}_{ws} of the mineral dust RMs. The elemental concentration of Cu in the dust RMs is lower than that of Fe by approximately three orders of magnitude (Figure S1 in Supporting Information S1), although no data indicating the solubility of Cu in mineral dusts are available. Because of the low elemental concentration of Cu in mineral dusts, the contribution of Cu ion to OP^{DTT}_{ws} is inferred as less important than that of Mn ion.

3.4. Mass-Normalized Oxidative Potential of the Mineral Dust RMs

The OP^{DTT} of aerosol particles is often presented as a mass-normalized value with a unit such as “picomoles DTT loss per minute per microgram of aerosol particles” because the scale is useful to compare intrinsic OP^{DTT}

across various aerosol samples. If OP^{DTT} is linear to the particle mass concentration in the DTT solution, then mass-normalized OP^{DTT} will not depend on the particle mass concentration. However, mass-normalized OP^{DTT} will vary depending on the particle concentration in the DTT solution when OP^{DTT} values are not linear to the particle concentration. As described in Section 3.2, neither OP^{DTT}_{total} nor OP^{DTT}_{ws} of the dust RMs were linear to the dust mass concentration (Figure 2). Consequently, as presented in Figure S2 in Supporting Information S1, mass-normalized OP^{DTT}_{total} and OP^{DTT}_{ws} of the dust RMs were not constant. Their values were dependent on the dust concentration in the DTT solution. For example, the mass-normalized OP^{DTT}_{total} of No. 30 decreased from approximately 18 to 4 pmol min⁻¹ μg⁻¹ when the mass concentration of No. 30 in the DTT solution increased from 10 to 500 μg mL⁻¹. When a large amount of mineral dust was included in the atmospheric aerosol sample, its mass-normalized OP^{DTT} must be evaluated carefully because it might change depending on the particle mass concentration added to the DTT solution.

To obtain robust measurements of mass-normalized OP^{DTT} of aerosol particles, Charrier et al. (2016) proposed measurement of the DTT loss rate at a standard particle concentration of 10 μg mL⁻¹ in the DTT solution in DTT assay. Mass-normalized OP^{DTT}_{total} values measured at 10 μg mL⁻¹ were approximately 18, 13, and 14 pmol min⁻¹ μg⁻¹, respectively, for No. 30, CJ-2, and ATD (Figure S2 in Supporting Information S1). In addition, OP^{DTT}_{total} was not measured for CJ-1 at 10 μg mL⁻¹ because its values were too low to measure. For CJ-1, the mass-normalized OP^{DTT}_{total} at 10 μg mL⁻¹ was estimated by extrapolation as 12 pmol min⁻¹ μg⁻¹.

Conte et al. (2017) reported mass-normalized OP^{DTT} of Saharan dust of less than 0.1 pmol min⁻¹ μg⁻¹ for both the water-soluble and insoluble fractions, which is less than one one-hundredth of the mass-normalized OP^{DTT} value obtained from this study for the dust RMs. To measure the OP^{DTT} value of Saharan dust, Conte et al. (2017) collected surface soil in Algeria and refined it by sieving at 100 μm. Although no size distribution of the Saharan dust sample has been presented in the relevant literature, it is presumably similar to that of CJ-1 because CJ-1 was also refined only by sieving, in this case by sieving at 150 μm (Nishikawa et al., 2000). Among the dust RMs examined for this study, CJ-1 was found to have the largest average particle size and the lowest SSA and OP^{DTT}. In addition, Conte et al. (2017) analyzed a Saharan dust sample at a concentration of 1,000 μg mL⁻¹ for DTT assay. This concentration is much higher than the particle concentrations analyzed in our study (10–500 μg mL⁻¹). Therefore, the low mass-normalized OP^{DTT} of Saharan dust reported by Conte et al. (2017) might be attributable to the large particle size and high particle concentration in DTT assay, although differences of their chemical and mineral components might partially explain the findings of low OP^{DTT}.

3.5. Estimation for Oxidative Potential of Mineral Dust Aerosols in the Atmosphere

As described in this section, we attempted to estimate OP^{DTT}_{total} values of mineral dust aerosols in the atmosphere using the relation between OP^{DTT}_{total} and the surface area of insoluble dust particles of Asian dust RMs (Figure 4a and Table 1). Often, the OP of atmospheric aerosols is measured for size-segregated particles such as fine and

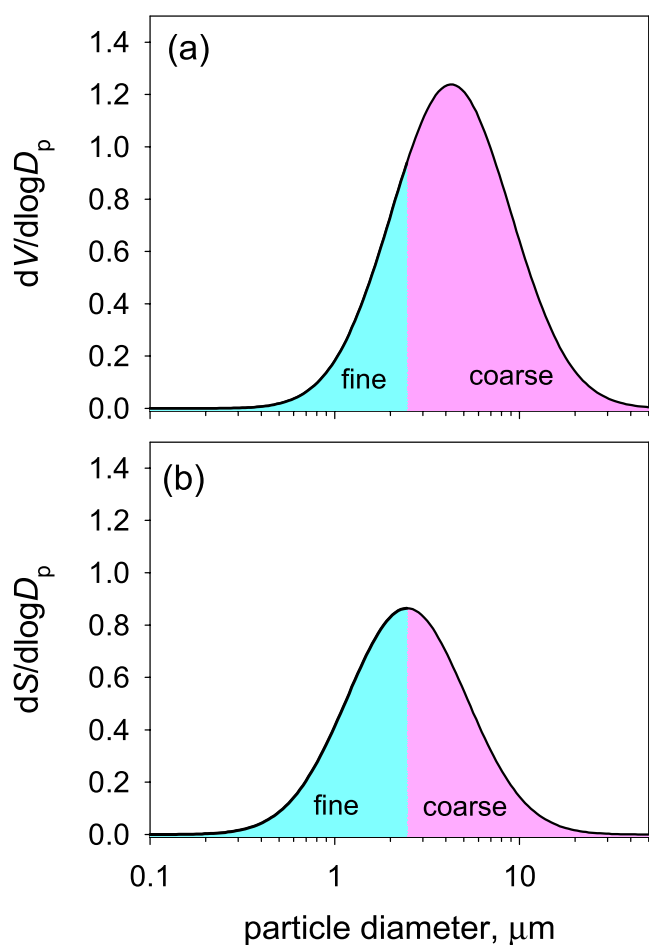


Figure 5. (a) Volume–size and (b) surface–size distributions of insoluble dust particles observed in an Asian dust plume in Kofu, Japan (Kobayashi et al., 2007). Both size distributions were normalized by the total volume. Areas shaded in pink and cyan respectively correspond to the total volume for (a) and total surface area for (b) of coarse and fine dust particles.

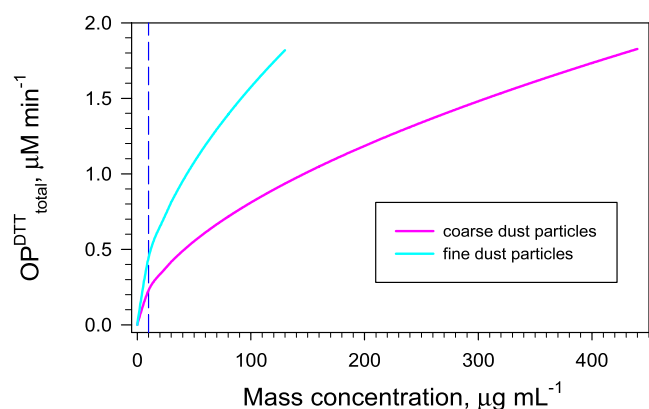


Figure 6. OP^{DTT}_{total} of fine and coarse dust particles estimated for a typical size distribution of long-range transported Asian dust aerosols. The blue dashed line represents dust mass concentration of $10 \mu\text{g mL}^{-1}$. The values of mass-normalized OP^{DTT}_{total} at $10 \mu\text{g mL}^{-1}$ were calculated from the DTT loss rates measured at this dust mass concentration.

coarse particles (Shiraiwa et al., 2017). Therefore, we estimated the OP^{DTT}_{total} of fine ($<2.5 \mu\text{m}$ diameter) and coarse ($>2.5 \mu\text{m}$ diameter) atmospheric dust particles. To estimate these values, we first estimated the SSA of fine and coarse dust particles assuming a typical size distribution of long-range transported Asian dust aerosols observed in Japan. Then, using the estimated SSAs, we estimated OP^{DTT}_{total} of long-range transported atmospheric fine and coarse dust particles. Details of the estimates are explained below.

Volume (mass)–size distributions of desert dust aerosols show a dominant mode at $10\text{--}40 \mu\text{m}$ diameter at emission and near source regions (Hoffmann et al., 2008; Kok et al., 2017), which decreases concomitantly with increasing distance of transport because of the efficient deposition of the larger particles (Mahowald et al., 2014). In Japan, located more than $2,000\text{--}4,000 \text{ km}$ downwind from Asian dust source regions, the modal diameters in the volume (mass)–size distributions of Asian dust aerosols have been observed as approximately $2.5\text{--}5.6 \mu\text{m}$ diameter (Kobayashi et al., 2007; Mori et al., 2003; Quinn, 2004). For the present study, particularly addressing a long-range transported desert dust aerosol, we estimated its OP^{DTT}_{total} value assuming a size distribution of insoluble particles (Figure 5) equal to observed for an Asian dust plume in Kofu, Japan (Kobayashi et al., 2007). Figure 5a shows the volume–size distribution reported by Kobayashi et al. (2007) (mono-modal distribution with $D_{p,g} = 4.27 \mu\text{m}$ and $\sigma_g = 2.10$). Figure 5b shows the surface–size distribution calculated from the volume–size distribution assuming spherical particles. In dust plumes, the insoluble particles in this mode (coarse mode) are almost entirely mineral dust particles. From the volume–size and surface–size distributions presented in Figure 5, we calculated the total surface area to volume ratios (S_{total}/V_{total}) of fine and coarse dust particles. Using the S_{total}/V_{total} values, the SSAs of fine and coarse dust particles are obtainable following Equation 5 presented in Section 2.2. Assuming the density of quartz (2.65 g cm^{-3}), SSAs were estimated as 1.508 and $0.449 \text{ mm}^2 \mu\text{g}^{-1}$, respectively, for fine and coarse insoluble dust particles. By applying these SSA values and the relation between OP^{DTT}_{total} and insoluble particle surface area of Asian dust RMs (No. 30, CJ-1, and CJ-2) (Figure 4a), we estimated OP^{DTT}_{total} for fine and coarse dust particles as a function of their mass concentrations in the DTT solution.

Figure 6 shows the values of OP^{DTT}_{total} estimated for fine and coarse dust particles in a long-range transported Asian dust aerosol as a function of their mass concentration in the DTT solution. The values of mass-normalized OP^{DTT}_{total} at $10 \mu\text{g mL}^{-1}$ were estimated respectively as 44 and $23 \text{ pmol min}^{-1} \mu\text{g}^{-1}$ for fine and coarse dust particles. These values are quite consistent with the mass-normalized OP^{DTT}_{total} of atmospheric aerosols observed during Asian dust events in Fukuoka, Japan (47 and $21 \text{ pmol min}^{-1} \mu\text{g}^{-1}$, respectively, for fine and coarse particles, on average) (Nishita-Hara et al., 2019), suggesting that aging of mineral dust particles by chemical processing in the atmosphere does not critically affect their mass-normalized OP^{DTT}_{total} . Only particle size reduction might be the primary factor causing a significant change of the mass-normalized OP^{DTT}_{total} of mineral dust aerosols during atmospheric transport. The estimated values are also similar to the mass-normalized OP^{DTT}_{total} values observed during non-dust events in Fukuoka (45 and $25 \text{ pmol min}^{-1} \mu\text{g}^{-1}$, respectively, for fine and coarse particles, on average). The sampling site is in an urban residential area. For that reason, anthropogenic aerosols are dominant during non-dust events at the site. The results suggest that mass-normalized OP^{DTT}_{total} values of long-range transported Asian dust aerosols are almost equal to those of urban background aerosols.

Mineral dust plume advection might not dilute the OP^{DTT} value of urban aerosols. It might cause a marked increase in human exposure to redox-active aerosols.

The mass-normalized OP^{DTT}_{total} value estimated for the fine dust particles ($44 \text{ pmol min}^{-1} \mu\text{g}^{-1}$) was two times higher than that estimated for the coarse dust particles ($23 \text{ pmol min}^{-1} \mu\text{g}^{-1}$). However, because the atmospheric volume (mass) concentration of the coarse dust particles is approximately three times higher than that of the fine dust particles (Figure 5a), the air-volume-normalized OP^{DTT}_{total} is still higher for the coarse dust particles than for the fine dust particles. Moreover, in the whole respiratory tract, deposition is much more effective for the coarse particles than for the fine particles (Hyder et al., 1986). Therefore, in the whole respiratory tract, coarse dust particles might contribute much more to the total exposure amount to DTT-active substances than the fine dust particles contribute. In the alveolar region, fine particles with $0.1\text{--}2.5 \mu\text{m}$ diameter have comparable deposition to that of coarse particles (Hyder et al., 1986). Therefore, regarding health effects occurring through deposition in the lungs, the fine dust particles can be as important as the coarse dust particles.

4. Summary and Conclusions

We evaluated the OP^{DTT} values of the total and water-soluble fractions of four mineral dust RMs with different particle size distributions. Findings obtained from this study indicate that both water-soluble and insoluble fractions of mineral dust particles contribute greatly to OP^{DTT} , suggesting that not only water-soluble transition metals but also the surfaces of insoluble mineral particles contribute considerably to the OP^{DTT} of mineral dust aerosols. Mass-normalized OP^{DTT} values differ depending on the dust RMs. However, the DTT loss rates normalized by the surface area of insoluble dust particles show good agreement among the dust RMs, indicating the insoluble particle surface area as a crucially important controlling factor for OP^{DTT} of mineral dust aerosols. During atmospheric transport, the SSA of mineral dust particles increases gradually because larger mineral dust particles are removed preferentially from the atmosphere. Consequently, the mass-normalized OP^{DTT} of atmospheric mineral dust aerosols might increase during atmospheric transport while the atmospheric dust burden decreases. Based on the relation between OP^{DTT} values of the Asian dust RMs and surface area of insoluble dust particles, we estimated the OP^{DTT} of fine and coarse dust particles assuming a typical size distribution of insoluble dust particles observed in Asian dust aerosols transported for thousands of kilometers. The mass-normalized OP^{DTT} values were estimated as 44 and $23 \text{ pmol min}^{-1} \mu\text{g}^{-1}$, respectively, for the fine and coarse dust particles. Those findings are quite consistent with those observed during both Asian dust events and non-dust periods at an urban background site in Japan. The results suggest that the mass-normalized OP^{DTT} of long-range transported atmospheric mineral dust aerosols are almost identical to those of urban background aerosols. Mineral dust plume advection might not necessarily dilute OP^{DTT} of urban aerosols, but it might cause a marked increase in human exposure to redox-active aerosols, even in areas that are far downwind from mineral dust source regions.

Conflict of Interest

The authors declare no conflicts of interest relevant to this study.

Data Availability Statement

The data presented in this report are available at figshare.com (<https://figshare.com/s/f77889d7ee7e9044eb2b>).

Acknowledgments

The authors are grateful to M. Nishikawa for the use of certified Asian dust reference materials. This work was supported by the Steel Foundation for Environmental Protection Technology Grants (16taiki-240, 19taiki-265), JSPS KAKENHI Grant (15K12219), the Environment Research and Technology Development Fund (JPMEERF20205007) of the Environmental Restoration and Conservation Agency of Japan, and Academia, Industry and Government Collaborative Research Organization (963, Fukuoka Institute for Atmospheric Environment and Health) of Fukuoka University.

References

- Aghababaeian, H., Ostadtaghizadeh, A., Ardalani, A., Asgary, A., Akbary, M., Yekaninejad, M. S., & Stephens, C. (2021). Global health impacts of dust storms: A systematic review. *Environmental Health Insights*, *15*, 1–28. <https://doi.org/10.1177/11786302211018390>
- Baker, A. R., & Jickells, T. D. (2006). Mineral particle size as a control on aerosol iron solubility. *Geophysical Research Letters*, *33*(17), L17608. <https://doi.org/10.1029/2006GL026557>
- Baker, A. R., Jickells, T. D., Witt, M., & Linge, K. L. (2006). Trends in the solubility of iron, aluminium, manganese and phosphorus in aerosol collected over the Atlantic Ocean. *Marine Chemistry*, *98*(1), 43–58. <https://doi.org/10.1016/j.marchem.2005.06.004>
- Bates, J. T., Fang, T., Verma, V., Zeng, L., Weber, R. J., Tolbert, P. E., et al. (2019). Review of acellular assays of ambient particulate matter oxidative potential: Methods and relationships with composition, sources, and health effects. *Environmental Science and Technology*, *53*(8), 4003–4019. <https://doi.org/10.1021/acs.est.8b03430>
- Broadley, S. L., Murray, B. J., Herbert, R. J., Atkinson, J. D., Dobbie, S., Malkin, T. L., et al. (2012). Immersion mode heterogeneous ice nucleation by an illite rich powder representative of atmospheric mineral dust. *Atmospheric Chemistry and Physics*, *12*(1), 287–307. <https://doi.org/10.5194/acp-12-287-2012>

- Caquineau, S., Gaudichet, A., Gomes, L., Magonthier, M.-C., & Chatenet, B. (1998). Saharan dust: Clay ratio as a relevant tracer to assess the origin of soil-derived aerosols. *Geophysical Research Letters*, 25(7), 983–986. <https://doi.org/10.1029/98gl00569>
- Charrier, J. G., & Anastasio, C. (2012). On dithiothreitol (DTT) as a measure of oxidative potential for ambient particles: Evidence for the importance of soluble transition metals. *Atmospheric Chemistry and Physics*, 12(19), 9321–9333. <https://doi.org/10.5194/acp-12-9321-2012>
- Charrier, J. G., McFall, A. S., Vu, K. K., Baroi, J., Olea, C., Hasson, A., & Anastasio, C. (2016). A bias in the “mass-normalized” DTT response—An effect of non-linear concentration-response curves for copper and manganese. *Atmospheric Environment*, 144, 325–334. <https://doi.org/10.1016/j.atmosenv.2016.08.071>
- Cho, A. K., Sioutas, C., Miguel, A. H., Kumagai, Y., Schmitz, D. A., Singh, M., et al. (2005). Redox activity of airborne particulate matter at different sites in the Los Angeles Basin. *Environmental Research*, 99(1), 40–47. <https://doi.org/10.1016/j.envres.2005.01.003>
- Conte, E., Canepari, S., Frasca, D., & Simonetti, G. (2017). Oxidative potential of selected PM components. *Proceedings*, 1(5), 108. <https://doi.org/10.3390/ecas2017-04131>
- de Longueville, F., Ozer, P., Doumbia, S., & Henry, S. (2013). Desert dust impacts on human health: An alarming worldwide reality and a need for studies in West Africa. *International Journal of Biometeorology*, 57(1), 1–19. <https://doi.org/10.1007/s00484-012-0541-y>
- Eyer, P., Worek, F., Kiderlen, D., Sinko, G., Stuglin, A., Simeon-Rudolf, V., & Reiner, E. (2003). Molar absorption coefficients for the reduced Ellman reagent: Reassessment. *Analytical Biochemistry*, 312(2), 224–227. [https://doi.org/10.1016/S0003-2697\(02\)00506-7](https://doi.org/10.1016/S0003-2697(02)00506-7)
- Falkovich, A. H., Schkolnik, G., Ganor, E., & Rudich, Y. (2004). Adsorption of organic compounds pertinent to urban environments onto mineral dust particles. *Journal of Geophysical Research*, 109(D2), D02208. <https://doi.org/10.1029/2003JD003919>
- Formenti, P., Caquineau, S., Chevaillier, S., Klaver, A., Desboeufs, K., Rajot, J. L., et al. (2014). Dominance of goethite over hematite in iron oxides of mineral dust from Western Africa: Quantitative partitioning by X-ray absorption spectroscopy. *Journal of Geophysical Research: Atmospheres*, 119(22), 12740–12754. <https://doi.org/10.1002/2014jd021668>
- Formenti, P., Schütz, L., Balkanski, Y., Desboeufs, K., Ebert, M., Kandler, K., et al. (2011). Recent progress in understanding physical and chemical properties of African and Asian mineral dust. *Atmospheric Chemistry and Physics*, 11(16), 8231–8256. <https://doi.org/10.5194/acp-11-8231-2011>
- Fussell, J. C., & Kelly, F. J. (2021). Mechanisms underlying the health effects of desert sand dust. *Environment International*, 157, 106790. <https://doi.org/10.1016/j.envint.2021.106790>
- Ginoux, P., Prospero, J. M., Gill, T. E., Hsu, N. C., & Zhao, M. (2012). Global-scale attribution of anthropogenic and natural dust sources and their emission rates based on MODIS Deep Blue aerosol products. *Reviews of Geophysics*, 50(3), RG3005. <https://doi.org/10.1029/2012rg000388>
- Goudie, A. S. (2014). Desert dust and human health disorders. *Environment International*, 63, 101–113. <https://doi.org/10.1016/j.envint.2013.10.011>
- Grousset, F. E., Ginoux, P., Bory, A., & Biscaye, P. E. (2003). Case study of a Chinese dust plume reaching the French Alps. *Geophysical Research Letters*, 30(6), 1277. <https://doi.org/10.1029/2002gl016833>
- Hashizume, M., Kim, Y., Ng, C. F. S., Chung, Y., Madaniyazi, L., Bell, M. L., et al. (2020). Health effects of Asian dust: A systematic review and meta-analysis. *Environmental Health Perspectives*, 128(6), 66001. <https://doi.org/10.1289/EHP5312>
- Hashizume, M., Ueda, K., Nishiwaki, Y., Michikawa, T., & Onozuka, D. (2010). Health effects of Asian dust events: A review of the literature (in Japanese with English abstract). *Nihon Eiseigaku Zasshi*, 65(3), 413–421. <https://doi.org/10.1265/jjh.65.413>
- He, M., Ichinose, T., Yoshida, S., Nishikawa, M., Sun, G., & Shibamoto, T. (2019). Role of iron and oxidative stress in the exacerbation of allergic inflammation in murine lungs caused by urban particulate matter < 2.5 μm and desert dust. *Journal of Applied Toxicology*, 39(6), 855–867. <https://doi.org/10.1002/jat.3773>
- Heyder, J., Gebhart, J., Rudolf, G., Schiller, C. F., & Stahlhofen, W. (1986). Deposition of particles in the human respiratory tract in the size range 0.005–15 μm. *Journal of Aerosol Science*, 17(5), 811–825. [https://doi.org/10.1016/0021-8502\(86\)90035-2](https://doi.org/10.1016/0021-8502(86)90035-2)
- Higashisaka, K., Fujimura, M., Taira, M., Yoshida, T., Tsunoda, S.-i., Baba, T., et al. (2014). Asian dust particles induce macrophage inflammatory responses via mitogen-activated protein Kinase activation and reactive oxygen species production. *Journal of Immunology Research*, 2014, 856154–856159. <https://doi.org/10.1155/2014/856154>
- Hiyoshi, K., Ichinose, T., Sadakane, K., Takano, H., Nishikawa, M., Mori, I., et al. (2005). Asian sand dust enhances ovalbumin-induced eosinophil recruitment in the alveoli and airway of mice. *Environmental Research*, 99(3), 361–368. <https://doi.org/10.1016/j.envres.2005.03.008>
- Hoffmann, C., Funk, R., Sommer, M., & Li, Y. (2008). Temporal variations in PM10 and particle size distribution during Asian dust storms in Inner Mongolia. *Atmospheric Environment*, 42(36), 8422–8431. <https://doi.org/10.1016/j.atmosenv.2008.08.014>
- Ichinose, T., Yoshida, S., Sadakane, K., Takano, H., Yanagisawa, R., Inoue, K., et al. (2008). Effects of Asian sand dust, Arizona sand dust, amorphous silica and aluminum oxide on allergic inflammation in the murine lung. *Inhalation Toxicology*, 20(7), 685–694. <https://doi.org/10.1080/08958370801935133>
- Jeong, G. Y. (2008). Bulk and single-particle mineralogy of Asian dust and a comparison with its source soils. *Journal of Geophysical Research*, 113(D2), D02208. <https://doi.org/10.1029/2007jd008606>
- Jeong, G. Y., Kim, J. Y., Seo, J., Kim, G. M., Jin, H. C., & Chun, Y. (2014). Long-range transport of giant particles in Asian dust identified by physical, mineralogical, and meteorological analysis. *Atmospheric Chemistry and Physics*, 14(1), 505–521. <https://doi.org/10.5194/acp-14-505-2014>
- Jiang, H. H., Ahmed, C. M. S., Canchola, A., Chen, J. Y., & Lin, Y. H. (2019). Use of dithiothreitol assay to evaluate the oxidative potential of atmospheric aerosols. *Atmosphere*, 10(10), 571. <https://doi.org/10.3390/atmos10100571>
- Jickells, T. D., An, Z. S., Andersen, K. K., Baker, A. R., Bergametti, G., Brooks, N., et al. (2005). Global iron connections between desert dust, ocean biogeochemistry, and climate. *Science*, 308(5718), 67–71. <https://doi.org/10.1126/science.1105959>
- Kachur, A. V., Held, K. D., Koch, C. J., & Biaglow, J. E. (1997). Mechanism of production of hydroxyl radicals in the copper-catalyzed oxidation of dithiothreitol. *Radiation Research*, 147(4), 409–415. <https://doi.org/10.2307/3579496>
- Kameda, T., Azumi, E., Fukushima, A., Tang, N., Matsuki, A., Kamiya, Y., et al. (2016). Mineral dust aerosols promote the formation of toxic nitropolycyclic aromatic compounds. *Scientific Reports*, 6(1), 24427. <https://doi.org/10.1038/srep24427>
- Kanji, Z. A., & Abbatt, J. P. (2010). Ice nucleation onto Arizona test dust at cirrus temperatures: Effect of temperature and aerosol size on onset relative humidity. *Journal of Physical Chemistry A*, 114(2), 935–941. <https://doi.org/10.1021/jp908661m>
- Karanasiou, A., Moreno, N., Moreno, T., Viana, M., de Leeuw, F., & Querol, X. (2012). Health effects from Sahara dust episodes in Europe: Literature review and research gaps. *Environment International*, 47, 107–114. <https://doi.org/10.1016/j.envint.2012.06.012>
- Kobayashi, H., Arai, K., Murayama, T., Iokibe, K., Koga, R., & Shiobara, M. (2007). High-resolution measurement of size distributions of Asian dust using a coulter multisizer. *Journal of Atmospheric and Oceanic Technology*, 24(2), 194–205. <https://doi.org/10.1175/Jtech1965.1>
- Kok, J. F., Adebisi, A. A., Albani, S., Balkanski, Y., Checa-Garcia, R., Chin, M. A., et al. (2021). Contribution of the world's main dust source regions to the global cycle of desert dust. *Atmospheric Chemistry and Physics*, 21(10), 8169–8193. <https://doi.org/10.5194/acp-21-8169-2021>

- Kok, J. F., Ridley, D. A., Zhou, Q., Miller, R. L., Zhao, C., Heald, C. L., et al. (2017). Integrative analysis of desert dust size and abundance suggests less dust climate cooling. *Nature Geoscience*, 10(4), 274–278. <https://doi.org/10.1038/ngeo2912>
- Kotsyfakis, M., Zarogiannis, S. G., & Patelarou, E. (2019). The health impact of Saharan dust exposure. *International Journal of Occupational Medicine & Environmental Health*, 32(6), 749–760. <https://doi.org/10.13075/ijomeh.1896.01466>
- Kumagai, Y., Koide, S., Taguchi, K., Endo, A., Nakai, Y., Yoshikawa, T., & Shimojo, N. (2002). Oxidation of proximal protein sulfhydryls by phenanthraquinone, a component of diesel exhaust particles. *Chemical Research in Toxicology*, 15(4), 483–489. <https://doi.org/10.1021/tx100993>
- Kyung, S. Y., Yoon, J. Y., Kim, Y. J., Lee, S. P., Park, J. W., & Jeong, S. H. (2012). Asian dust particles induce TGF-beta(1) via reactive oxygen species in bronchial epithelial cells. *Tuberculosis and Respiratory Diseases*, 73(2), 84–92. <https://doi.org/10.4046/trd.2012.73.2.84>
- Li, Q. F., Wyatt, A., & Kamens, R. M. (2009). Oxidant generation and toxicity enhancement of aged-diesel exhaust. *Atmospheric Environment*, 43(5), 1037–1042. <https://doi.org/10.1016/j.atmosenv.2008.11.018>
- Liu, Q., Baumgartner, J., Zhang, Y., Liu, Y., Sun, Y., & Zhang, M. (2014). Oxidative potential and inflammatory impacts of source apportioned ambient air pollution in Beijing. *Environmental Science and Technology*, 48(21), 12920–12929. <https://doi.org/10.1021/es5029876>
- Liu, Q., Zhang, Y., Liu, Y., & Zhang, M. (2014). Characterization of springtime airborne particulate matter-bound reactive oxygen species in Beijing. *Environmental Science and Pollution Research International*, 21(15), 9325–9333. <https://doi.org/10.1007/s11356-014-2843-6>
- Liu, W., Xu, Y., Liu, W., Liu, Q., Yu, S., Liu, Y., et al. (2018). Oxidative potential of ambient PM_{2.5} in the coastal cities of the Bohai Sea, northern China: Seasonal variation and source apportionment. *Environmental Pollution*, 236, 514–528. <https://doi.org/10.1016/j.envpol.2018.01.116>
- Mahowald, N., Albani, S., Kok, J. F., Engelstaeder, S., Scanza, R., Ward, D. S., & Flanner, M. G. (2014). The size distribution of desert dust aerosols and its impact on the Earth system. *Aeolian Research*, 15, 53–71. <https://doi.org/10.1016/j.aeolia.2013.09.002>
- Mahowald, N., Kohfeld, K., Hansson, M., Balkanski, Y., Harrison, S. P., Prentice, I. C., et al. (1999). Dust sources and deposition during the last glacial maximum and current climate: A comparison of model results with paleodata from ice cores and marine sediments. *Journal of Geophysical Research*, 104(D13), 15895–15916. <https://doi.org/10.1029/1999JD900084>
- Mahowald, N. M., Hamilton, D. S., Mackey, K. R. M., Moore, J. K., Baker, A. R., Scanza, R. A., & Zhang, Y. (2018). Aerosol trace metal leaching and impacts on marine microorganisms. *Nature Communications*, 9(1), 2614. <https://doi.org/10.1038/s41467-018-04970-7>
- McKendry, I. G., Strawbridge, K. B., O'Neill, N. T., Macdonald, A. M., Liu, P. S. K., Leaitch, W. R., et al. (2007). Trans-pacific transport of Saharan dust to western North America: A case study. *Journal of Geophysical Research*, 112(D1), D01103. <https://doi.org/10.1029/2006jd007129>
- McNaughton, C. S., Clarke, A. D., Howell, S. G., Pinkerton, M., Anderson, B., Thornhill, L., et al. (2007). Results from the DC-8 inlet characterization experiment (DICE): Airborne versus surface sampling of mineral dust and sea salt aerosols. *Aerosol Science and Technology*, 41(2), 136–159. <https://doi.org/10.1080/02786820601118406>
- Möhler, O., Field, P. R., Connolly, P., Benz, S., Saathoff, H., Schnaiter, M., et al. (2006). Efficiency of the deposition mode ice nucleation on mineral dust particles. *Atmospheric Chemistry and Physics*, 6(10), 3007–3021. <https://doi.org/10.5194/acp-6-3007-2006>
- Mori, I., Nishikawa, M., Tanimura, T., & Quan, H. (2003). Change in size distribution and chemical composition of kosa (Asian dust) aerosol during long-range transport. *Atmospheric Environment*, 37(30), 4253–4263. [https://doi.org/10.1016/S1352-2310\(03\)00535-1](https://doi.org/10.1016/S1352-2310(03)00535-1)
- Nicolas, J., Jaafar, M., Sepetdjian, E., Saad, W., Sioutas, C., Shihadeh, A., & Saliba, N. A. (2015). Redox activity and chemical interactions of metal oxide Nano- and microparticles with dithiothreitol (DTT). *Environmental Science Processes & Impacts*, 17(11), 1952–1958. <https://doi.org/10.1039/c5em00352k>
- Nishikawa, M., Batdorj, D., Ukachi, M., Onishi, K., Nagano, K., Mori, I., et al. (2013). Preparation and chemical characterisation of an Asian mineral dust certified reference material. *Analytical Methods*, 5(16), 4088–4095. <https://doi.org/10.1039/c3ay40435h>
- Nishikawa, M., Hao, Q., & Morita, M. (2000). Preparation and evaluation of certified reference materials for Asian mineral dust. *Global Environmental Research*, 4(1), 103–113.
- Nishita-Hara, C., Hirabayashi, M., Hara, K., Yamazaki, A., & Hayashi, M. (2019). Dithiothreitol-measured oxidative potential of size-segregated particulate matter in Fukuoka, Japan: Effects of Asian dust events. *GeoHealth*, 3(6), 160–173. <https://doi.org/10.1029/2019GH000189>
- Ooki, A., Nishioka, J., Ono, T., & Noriki, S. (2009). Size dependence of iron solubility of Asian mineral dust particles. *Journal of Geophysical Research*, 114(D3), D03202. <https://doi.org/10.1029/2008jd010804>
- Osada, K. (2013). Water soluble fraction of Asian dust particles. *Atmospheric Research*, 124, 101–108. <https://doi.org/10.1016/j.atmosres.2013.01.001>
- Pardo, M., Katra, I., Schauer, J. J., & Rudich, Y. (2017). Mitochondria-mediated oxidative stress induced by desert dust in rat alveolar macrophages. *GeoHealth*, 1(1), 4–16. <https://doi.org/10.1002/2016GH000017>
- Park, J., Jang, M., & Yu, Z. (2017). Heterogeneous photo-oxidation of SO₂ in the presence of two different mineral dust particles: Gobi and Arizona dust. *Environmental Science and Technology*, 51(17), 9605–9613. <https://doi.org/10.1021/acs.est.7b00588>
- Prospero, J. M., Ginoux, P., Torres, O., Nicholson, S. E., & Gill, T. E. (2002). Environmental characterization of global sources of atmospheric soil dust identified with the Nimbus 7 Total Ozone Mapping Spectrometer (TOMS) absorbing aerosol product. *Reviews of Geophysics*, 40(1), 1002–2–31. <https://doi.org/10.1029/2000rg000095>
- Quinn, P. K. (2004). Aerosol optical properties measured onboard the Ronald H. Brown during ACE-Asia as a function of aerosol chemical composition and source region. *Journal of Geophysical Research*, 109(D19), D19S01. <https://doi.org/10.1029/2003jd004010>
- Sakai, T., Nagai, T., Zaizen, Y., & Mano, Y. (2010). Backscattering linear depolarization ratio measurements of mineral, sea-salt, and ammonium sulfate particles simulated in a laboratory chamber. *Applied Optics*, 49(23), 4441–4449. <https://doi.org/10.1364/AO.49.004441>
- Schoonen, M. A. A., Cohn, C. A., Roemer, E., Laffers, R., Simon, S. R., & O'Riordan, T. (2006). Mineral-induced formation of reactive oxygen species. *Medical Mineralogy and Geochemistry*, 64(1), 179–221. <https://doi.org/10.2138/rmg.2006.64.7>
- Shi, Z. B., Woodhouse, M. T., Carslaw, K. S., Krom, M. D., Mann, G. W., Baker, A. R., et al. (2011). Minor effect of physical size sorting on iron solubility of transported mineral dust. *Atmospheric Chemistry and Physics*, 11(16), 8459–8469. <https://doi.org/10.5194/acp-11-8459-2011>
- Shiraiva, M., Ueda, K., Pozzer, A., Lammel, G., Kampf, C. J., Fushimi, A., et al. (2017). Aerosol health effects from molecular to global scales. *Environmental Science and Technology*, 51(23), 13545–13567. <https://doi.org/10.1021/acs.est.7b04417>
- Sokolik, I. N., & Toon, O. B. (1999). Incorporation of mineralogical composition into models of the radiative properties of mineral aerosol from UV to IR wavelengths. *Journal of Geophysical Research*, 104(D8), 9423–9444. <https://doi.org/10.1029/1998jd200048>
- Stanelle, T., Bey, I., Raddatz, T., Reick, C., & Tegen, I. (2014). Anthropogenically induced changes in twentieth century mineral dust burden and the associated impact on radiative forcing. *Journal of Geophysical Research – Atmospheres*, 119(23), 13526–13546. <https://doi.org/10.1002/2014JD022062>
- Tang, M. J., Schuster, G., & Crowley, J. N. (2014). Heterogeneous reaction of N₂O₃ with illite and Arizona test dust particles. *Atmospheric Chemistry and Physics*, 14(1), 245–254. <https://doi.org/10.5194/acp-14-245-2014>
- Textor, C., Schulz, M., Guibert, S., Kinne, S., Balkanski, Y., Bauer, S., et al. (2006). Analysis and quantification of the diversities of aerosol life cycles within AeroCom. *Atmospheric Chemistry and Physics*, 6(7), 1777–1813. <https://doi.org/10.5194/acp-6-1777-2006>

- Trochkin, D., Iwasaka, Y., Matsuki, A., Yamada, M., Kim, Y.-S., Nagatani, T., et al. (2003). Mineral aerosol particles collected in Dunhuang, China, and their comparison with chemically modified particles collected over Japan. *Journal of Geophysical Research*, *108*(D23), 8642. <https://doi.org/10.1029/2002JD003268>
- Uno, I., Eguchi, K., Yumimoto, K., Takemura, T., Shimizu, A., Uematsu, M., et al. (2009). Asian dust transported one full circuit around the globe. *Nature Geoscience*, *2*(8), 557–560. <https://doi.org/10.1038/Ngeo583>
- Veghte, D. P., Altaf, M. B., Haines, J. D., & Freedman, M. A. (2016). Optical properties of non-absorbing mineral dust components and mixtures. *Aerosol Science and Technology*, *50*(11), 1239–1252. <https://doi.org/10.1080/02786826.2016.1225153>
- Yabuki, S., Kanayama, S., & Honda, M. (2002). Oudo hyoujunbusshitsu(CJ1) oyobi kousa earozoru hyoujunbusshitsu(CJ2) no koubutsu sosei (tokushu kosa) (in Japanese). *Global Environmental Research*, *7*(2), 171–179.
- Yamashita, K., Murakami, M., Hashimoto, A., & Tajiri, T. (2011). CCN Ability of Asian mineral dust particles and their effects on cloud Droplet formation. *Journal of the Meteorological Society of Japan*, *89*(5), 581–587. <https://doi.org/10.2151/jmsj.2011-512>
- Yu, S., Liu, W., Xu, Y., Yi, K., Zhou, M., Tao, S., & Liu, W. (2019). Characteristics and oxidative potential of atmospheric PM_{2.5} in Beijing: Source apportionment and seasonal variation. *Science of the Total Environment*, *650*(Pt 1), 277–287. <https://doi.org/10.1016/j.scitotenv.2018.09.021>
- Zhang, D., Shi, G.-Y., Iwasaka, Y., & Hu, M. (2000). Mixture of sulfate and nitrate in coastal atmospheric aerosols: Individual particle studies in Qingdao (36°047'N, 120°21'E), China. *Atmospheric Environment*, *34*(17), 2669–2679. [https://doi.org/10.1016/S1352-2310\(00\)00078-9](https://doi.org/10.1016/S1352-2310(00)00078-9)
- Zhang, X. L., Zhao, L. J., Tong, D. Q., Wu, G. J., Dan, M., & Teng, B. (2016). A systematic review of global desert dust and associated human health effects. *Atmosphere*, *7*(12), 158. <https://doi.org/10.3390/atmos7120158>